

Inductive Source Induced Polarization

David Marchant

UBC-Geophysical Inversion Facility
Dept Earth and Ocean Science,
6339 Stores Road,
Vancouver, V6T1Z4 dmarchant@eos.ubc.ca

Eldad Haber

UBC-Geophysical Inversion Facility
Dept Earth and Ocean Science,
6339 Stores Road,
Vancouver, V6T1Z4 haber@math.ubc.ca

Douglas W Oldenburg

UBC-Geophysical Inversion Facility
Dept Earth and Ocean Science,
6339 Stores Road,
Vancouver, V6T1Z4 doug@eos.ubc.ca

SUMMARY

We present a new survey methodology to map the distribution of chargeable material in the subsurface using inductive electromagnetic sources and observations of the magnetic fields in the frequency domain. An accompanying inversion algorithm is developed, and the technique is tested on synthetic data.

Key words: Induced polarization, Electromagnetics, Geophysical Inversion

INTRODUCTION

The presence of chargeable material in the ground can often provide an excellent proxy for the distribution of sulphides in the subsurface. Traditionally, chargeability is mapped using induced polarization (IP) surveys (Seigel, 1959) in which current is injected into the ground using two transmitter electrodes and the potential difference is measured across other pairs of electrodes placed away from the transmitter. These data are now commonly inverted to recover 2D or 3D chargeability structures (e.g. Oldenburg and Li (1994), Li and Oldenburg, (2000)).

Although IP methods have had great success, surveying large areas can be prohibitively time consuming and expensive. IP methods can also fail in some geological situations. If the surface material is too resistive it can be impossible to push enough current into the ground and to excite an observable polarization effect. In areas with very resistive overburden, the voltage and power limitations of the transmitter hardware adversely affect the resulting signal.

The magnetic induced polarization (MIP) method (Seigel, 1974) was developed in order to address these issues. In this method, the transmitter is still a grounded source but the secondary magnetic field is measured. A 3D inversion technique for MIP data was developed by Chen and Oldenburg (2003). MIP eliminates the time consuming task of placing receiver electrodes, but current still needs to be injected into the ground. The use of an inductive source was examined by Hohmann et al. (1970) and the use of natural sources was investigated by Gasperikova and Morrison (2001) but the method has not been developed for practical application.

In this work we propose a new inductive source IP (ISIP) technique. The technique is based on the ability to measure the differences in the magnetic fields at two low frequencies. We

propose a new way to process the data that is based on the character of the fields at low frequency accompanied with a new inversion methodology for an effective IP parameter.

METHOD

Maxwell's equations, in the frequency domain, assuming a time dependence of $e^{-i\omega t}$, are

$$\nabla \times \mathbf{E} - i\omega\mu\mathbf{H} = 0 \quad (1a)$$

$$\nabla \times \mathbf{H} - \sigma\mathbf{E} = \mathbf{s} \quad (1b)$$

Here, \mathbf{E} and \mathbf{H} are the electric and magnetic fields, σ is the conductivity and μ is magnetic susceptibility. If we define \mathbf{H} such that $\mathbf{H} = \mathbf{H}_0 + \mathbf{H}^s$ and $\nabla \times \mathbf{H}_0 = \mathbf{s}$ we can rewrite the equations in terms of \mathbf{E} and \mathbf{H}^s as

$$\nabla \times \mathbf{E} - i\omega\mu\mathbf{H}^s = i\omega\mu\mathbf{H}_0 \quad (2a)$$

$$\nabla \times \mathbf{H}^s - \sigma\mathbf{E} = 0 \quad (2b)$$

Eliminating \mathbf{E} from the system yields an equation for \mathbf{H}^s

$$\nabla \times \rho \nabla \times \mathbf{H}^s - i\omega\mu\mathbf{H}^s = i\omega\mu\mathbf{H}_0 \quad (3)$$

where ρ is the resistivity, $\rho = \frac{1}{\sigma}$. We first assume a real, non-dispersive (frequency independent) resistivity distribution ρ . Differentiating Equation 3 twice with respect to ω gives

$$\nabla \times \rho \nabla \times \frac{\partial \mathbf{H}^s}{\partial \omega} - i\omega\mu \frac{\partial \mathbf{H}^s}{\partial \omega} = i\mu(\mathbf{H}_0 + \mathbf{H}^s) \quad (4)$$

$$\nabla \times \rho \nabla \times \frac{\partial^2 \mathbf{H}^s}{\partial \omega^2} - i\omega\mu \frac{\partial^2 \mathbf{H}^s}{\partial \omega^2} = 2i\mu \frac{\partial \mathbf{H}^s}{\partial \omega} \quad (5)$$

Expanding \mathbf{H}^s about $\omega = 0$, and dropping the higher terms leaves

$$\mathbf{H}^s(\omega) \approx \left. \frac{\partial \mathbf{H}^s}{\partial \omega} \right|_{\omega=0} \omega + \left. \frac{1}{2} \frac{\partial^2 \mathbf{H}^s}{\partial \omega^2} \right|_{\omega=0} \omega^2 \quad (6)$$

We can see from Equations 4 and 5 that $\left. \frac{\partial \mathbf{H}^s}{\partial \omega} \right|_{\omega=0}$ is purely

imaginary, and that $\left. \frac{\partial^2 \mathbf{H}^s}{\partial \omega^2} \right|_{\omega=0}$ is purely real, giving

$$\Im(\mathbf{H}^s(\omega)) \approx \left. \frac{\partial \mathbf{H}^s}{\partial \omega} \right|_{\omega=0} \omega \quad \text{and} \quad \Re(\mathbf{H}^s(\omega)) \approx \left. \frac{1}{2} \frac{\partial^2 \mathbf{H}^s}{\partial \omega^2} \right|_{\omega=0} \omega^2.$$

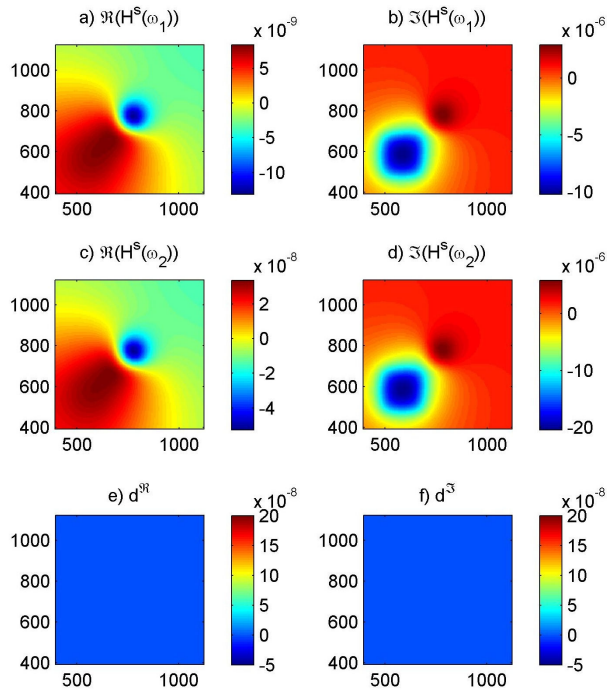


Figure 1. Secondary magnetic fields generated by a 100m loop centred at $x=600\text{m}$, $y=600\text{m}$ above a conductive (non-chargeable) block in a half space with $\omega_1 = 1\text{hz}$ and $\omega_2 = 2\text{hz}$. ISIP data (1e and 1f) show very little response to this model.

We define the quantities d^{\Re} and d^{\Im}

$$d^{\Re} = \Re(\mathbf{H}^s(\omega_2)) - \frac{\omega_2^2}{\omega_1^2} \Re(\mathbf{H}^s(\omega_1)) \quad (7a)$$

$$d^{\Im} = \Im(\mathbf{H}^s(\omega_2)) - \frac{\omega_2}{\omega_1} \Im(\mathbf{H}^s(\omega_1)) \quad (7b)$$

where ω_1 and ω_2 are two frequencies which are sufficiently low so that their inductive responses to a real conductivity earth are only minimally different, that is, we are working in resistive limit regime. For any real, non-dispersive resistivity distribution, we see from Equation 6 that both d^{\Re} and d^{\Im} should approximately equal zero. Signal in either of these quantities indicates the presence of chargeable material and we will use these data in our inversion.

Discretization

For numerical evaluation, we discretize Maxwell's equations on a orthogonal, staggered grid and use a finite volume approach (Haber and Ascher, 2001). If we assume that $\mu = \mu_0$, then $\nabla \cdot \mu \mathbf{H}^s = 0$. This is added as stabilization term to Equation 3 to yield

$$\nabla \times \rho \nabla \times \mathbf{H}^s - \nabla \rho \nabla \cdot \mu \mathbf{H}^s - i\omega \mu \mathbf{H}^s = i\omega \mu \mathbf{H}_0 \quad (8)$$

We choose to put \mathbf{H}^s on cell edges, and ρ at cell centres. Our matrix equations are

$$\left(\text{curl}^T \text{diag}(\mathbf{A}_v, \rho) \text{curl} + \text{grad} \text{diag}(\mathbf{A}_v, \rho) \text{grad}^T \mu - i\omega \mu \mathbf{I} \right) \mathbf{H}^s = i\omega \mu \mathbf{H}_0 \quad (9)$$

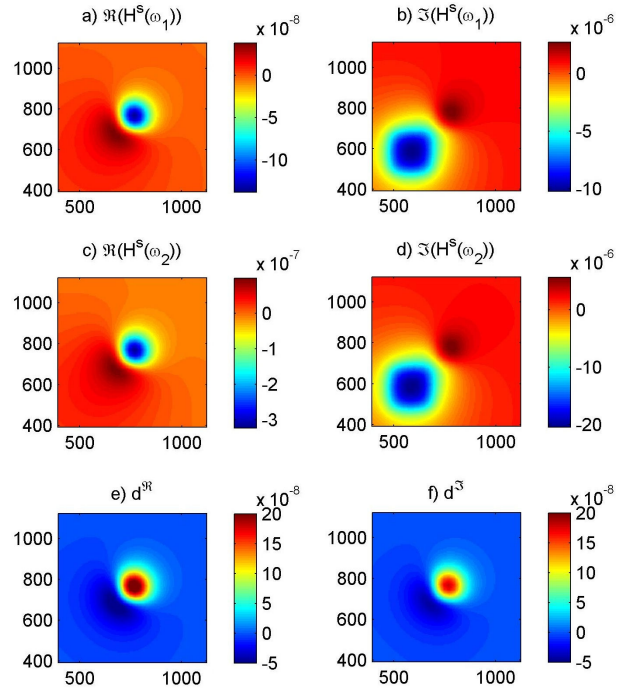


Figure 2. Secondary magnetic fields generated by a 100m loop centred at $x=600\text{m}$, $y=600\text{m}$ above a conductive block with a chargeability of 0.1.

where **curl** and **grad** are discrete forms of the curl and gradient operators, and \mathbf{A}_v is an averaging matrix.

To show the merits of our choice of data we perform a forward modelling. We use the Cole-Cole model (Pelton et al., 1978) to describe the complex resistivity. In the frequency domain

$$\rho(\omega) = \rho_0 \left(1 - \eta \left(1 - \frac{1}{1 + (i\omega\tau)^c} \right) \right) \quad (10)$$

where ρ_0 is the resistivity at zero frequency, η is the chargeability, and τ is a time constant. The parameter c is a constant which controls the frequency dependence of the material.

Figure 1 shows the vertical components of the secondary magnetic field computed using Equation 8. A square loop transmitter, 100m on a side, is centered at $x=600\text{m}$, $y=600\text{m}$, and is placed above a conductive ($2\ \Omega\text{m}$), non-chargeable block in a resistive halfspace (100 Ohm-m). Both the real and the imaginary components of the response are shown at 1 hz (ω_1) and 2 hz (ω_2). Figures 1e and 1f show the computed ISIP data. For this non-dispersive resistivity distribution, the values are approximately equal to zero.

Figure 2 shows results of an identical survey, but this time carried out above a chargeable block, with resistivities following a Cole-Cole model (Equation 10, $\rho_0 = 2\ \Omega\text{m}$, $\eta = 0.1$, $\tau = 0.1$, $c = 1$) In this case, there is strong dipolar signal observed in both the real and imaginary data as in Figures 2e and 2f. These are the data we will invert.

Formulating the ISIP data equations

The effect of chargeability is to cause a perturbation in the resistivity with frequency. Let ρ_1 equal the real, frequency independent, background conductivity. Let ρ_2 be the resistivity that would be observed at ω_2 . The frequencies ω_1 and ω_2 are closely spaced, so the resistivity that would be observed at ω_2 is equal to the resistivity at ω_1 , plus a small perturbation, or $\rho_2 = \rho_1 + \Delta\rho$. We can write

$$\mathbf{H}^s(\omega_2, \rho_2) \approx \mathbf{H}^s(\omega_2, \rho_1 + \Delta\rho) \approx \mathbf{H}^s(\omega_2, \rho_1) + \left. \frac{\partial \mathbf{H}^s}{\partial \rho} \right|_{\omega_2, \rho_1} \Delta\rho \quad (11)$$

Taking the Cole-Cole model, setting $c=1$, and expanding about $\omega=0$ gives

$$\rho(\omega) \approx \rho_0 - i\rho_0\eta\tau\omega \quad (12)$$

The first order perturbation is purely imaginary, so at low frequency $\Delta\rho$ is purely imaginary, which we can denote as $\Delta\rho_I$. Substituting this into Equation 11 and separating the real and the imaginary parts yields

$$\begin{aligned} \Re(\mathbf{H}^s(\omega_2, \rho_2)) &\approx \Re(\mathbf{H}^s(\omega_2, \rho_1)) + \left. \frac{\partial \Re \mathbf{H}^s}{\partial \rho_I} \right|_{\omega_2, \rho_1} \Delta\rho_I \\ &\approx \frac{\omega_2^2}{\omega_1^2} \Re(\mathbf{H}^s(\omega_1, \rho_1)) + \left. \frac{\partial \Re \mathbf{H}^s}{\partial \rho_I} \right|_{\omega_2, \rho_1} \Delta\rho_I \end{aligned} \quad (13a)$$

$$\begin{aligned} \Im(\mathbf{H}^s(\omega_2, \rho_2)) &\approx \Im(\mathbf{H}^s(\omega_2, \rho_1)) + \left. \frac{\partial \Im \mathbf{H}^s}{\partial \rho_I} \right|_{\omega_2, \rho_1} \Delta\rho_I \\ &\approx \frac{\omega_2}{\omega_1} \Im(\mathbf{H}^s(\omega_1, \rho_1)) + \left. \frac{\partial \Im \mathbf{H}^s}{\partial \rho_I} \right|_{\omega_2, \rho_1} \Delta\rho_I \end{aligned} \quad (13b)$$

Combining this with the equations for the ISIP data (Equation 7) leaves

$$d^{\Re} \approx \left. \frac{\partial \Re \mathbf{H}^s}{\partial \rho_I} \right|_{\omega_2, \rho_1} \Delta\rho \approx - \left. \frac{\partial \Re \mathbf{H}^s}{\partial \rho_I} \right|_{\omega_2, \rho_1} \rho_1 \eta \tau \omega_2 \quad (14a)$$

$$d^{\Im} \approx \left. \frac{\partial \Im \mathbf{H}^s}{\partial \rho_I} \right|_{\omega_2, \rho_1} \Delta\rho_I \approx - \left. \frac{\partial \Im \mathbf{H}^s}{\partial \rho_I} \right|_{\omega_2, \rho_1} \rho_1 \eta \tau \omega_2 \quad (14b)$$

To evaluate this we need to compute the sensitivities of \mathbf{H}^s to changes in the imaginary part of the resistivity. We define the operators \mathbf{T}_R and \mathbf{T}_I to be

$$\mathbf{T}_R = \mathbf{curl}^T \text{diag}(\mathbf{A}_v, \rho_R) \mathbf{curl} + \mathbf{grad} \text{diag}(\mathbf{A}_v, \rho_R) \mathbf{grad}^T \mu \quad (15a)$$

$$\mathbf{T}_I = \mathbf{curl}^T \text{diag}(\mathbf{A}_v, \rho_I) \mathbf{curl} + \mathbf{grad} \text{diag}(\mathbf{A}_v, \rho_I) \mathbf{grad}^T \mu \quad (15b)$$

Differentiating Equation 9 with respect to ρ_I , and separating the real and the imaginary parts gives

$$\mathbf{T}_R \frac{\partial \mathbf{H}_R^s}{\partial \rho_I} - (\mathbf{T}_I + \omega \mu \mathbf{I}) \frac{\partial \mathbf{H}_I^s}{\partial \rho_I} = \mathbf{curl}^T \text{diag}(\mathbf{curl} \mathbf{H}_I^s) \mathbf{A}_v \quad (16a)$$

$$(\mathbf{T}_I + \omega \mu \mathbf{I}) \frac{\partial \mathbf{H}_R^s}{\partial \rho_I} + \mathbf{T}_R \frac{\partial \mathbf{H}_I^s}{\partial \rho_I} = \mathbf{curl}^T \text{diag}(\mathbf{curl} \mathbf{H}_R^s) \mathbf{A}_v \quad (16b)$$

If we consider the sensitivity to changes in the imaginary part of the conductivity about a purely real conductivity, and we consider only low frequencies such that $\omega \mu \approx 0$ then this simplifies to

$$\mathbf{T}_R \frac{\partial \mathbf{H}_R^s}{\partial \rho_I} = \mathbf{curl}^T \text{diag}(\mathbf{curl} \mathbf{H}_I^s) \mathbf{A}_v \quad (17a)$$

$$\mathbf{T}_R \frac{\partial \mathbf{H}_I^s}{\partial \rho_I} = \mathbf{curl}^T \text{diag}(\mathbf{curl} \mathbf{H}_R^s) \mathbf{A}_v \quad (17b)$$

We can now define the quantities \mathbf{G}_I , \mathbf{G}_R and m to be

$$\mathbf{G}_I = -\omega_2 \mathbf{T}_R^{-1} \mathbf{curl}^T \text{diag}(\mathbf{curl} \mathbf{H}_I^s) \mathbf{A}_v \text{diag}(\rho_I) \quad (18a)$$

$$\mathbf{G}_R = -\omega_2 \mathbf{T}_R^{-1} \mathbf{curl}^T \text{diag}(\mathbf{curl} \mathbf{H}_R^s) \mathbf{A}_v \text{diag}(\rho_I) \quad (18b)$$

$$m = \eta \tau \quad (19)$$

this gives

$$d^{\Re} = \mathbf{G}_I m \quad (20a)$$

$$d^{\Im} = \mathbf{G}_R m \quad (20b)$$

The recovery of the ‘‘chargeability,’’ m , from the ISIP data therefore reduces to solving a standard linear inverse problem.

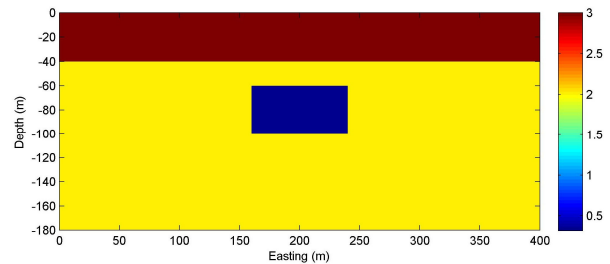


Figure 3. True resistivity model used in the synthetic test in $\log_{10} \Omega m$. The overburden is 40m thick and has a resistivity of $1000 \Omega m$ and the background is $100 \Omega m$. The block has a resistivity of $2 \Omega m$, a chargeability of 0.1, and time-constant of 0.1.

Inverse modelling

The goal of the inversion is to recover a chargeability distribution which can predict the observations while minimizing a predefined objective function. Prior to inverting for chargeability, we must have a real background resistivity, ρ_1 , from which to compute the sensitivity elements \mathbf{G}_I and \mathbf{G}_R . This background can be obtained by inverting the low frequency (ω_1) data from all transmitters and receivers if the data are sufficiently numerous. The desired sensitivities can be computed via Equation 18. The inverse problem is solved by minimizing the usual objective function $\phi = \phi_d + \beta \phi_m$ where ϕ_d is the data misfit, ϕ_m is a measure of the amount of structure present in the model and β is the regularization parameter. A Gauss-Newton procedure is used and the matrix system solved using Conjugate Gradient techniques. The

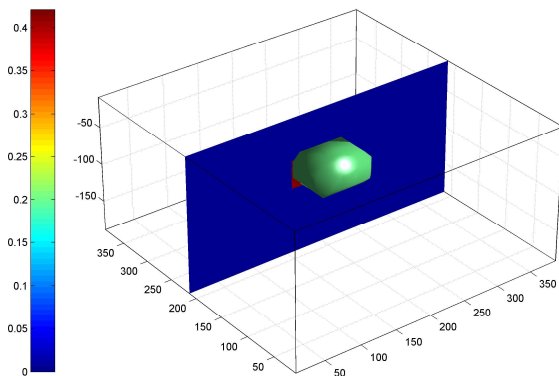


Figure 4. True chargeability distribution.

sensitivity is kept in factored form (Haber et al, 2004) with the forward modelling operator factored as a Cholesky decomposition. Positivity on the chargeability is achieved by implementing a projected gradient method. (Kelly, 1999).

Synthetic Example

A synthetic resistivity model was created containing a conductive, chargeable block ($\rho_0 = 2 \Omega m$, $\eta = 0.1$, $\tau = 0.1$, $c = 1$), buried beneath a resistive overburden ($1000 \Omega m$). The background had a resistivity of $100 \Omega m$. The resistive overburden was 40m thick. The block had dimensions of 80m on a side, with the top of the block being 60m below the surface. The synthetic resistivity model is shown in Figure 3.

The frequency domain response of this complex resistivity distribution was simulated for 9 square loop transmitters. The transmitters were on the surface, were 50m on a side, and were distributed as a 3 by 3 grid. A grid of 64 receivers (placed every 40m, 1m above the surface) recorded the three components of the magnetic field. Data were modelled at 1hz and 2hz. The real, synthetic ISIP data were then calculated using Equation 7a.

The ISIP data were contaminated with normally distributed, random noise prior to inversion. The noise had a standard deviation of 5% of the data value plus a small floor. The data were then inverted using the methodology presented previously. The true and resulting chargeability models are shown in Figures 4 and 5.

Conclusion

In this work we have explored a new imaging technique to recover the distribution of chargeable material in the earth given a magnetic sources and magnetic receivers. Our method is based on low frequency measurements so that the inductive responses to a real conductivity distribution are minimally different at the two frequencies. That is, we are working in the resistive limit regime. We have developed a mathematical framework and applied it to synthetic data set that demonstrates the potential of the method.

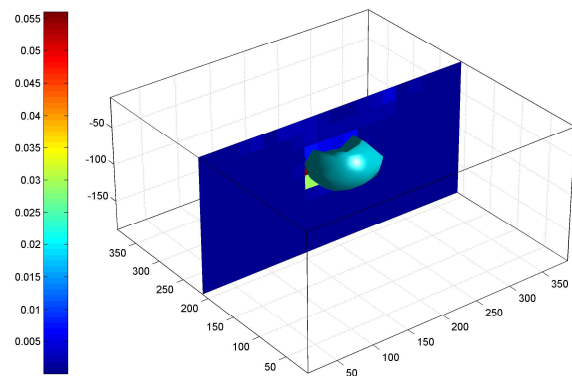


Figure 5. Chargeability distribution recovered from inversion of synthetic data.

REFERENCES

- Chen, J. and Oldenburg, D. W., 2003, 3-D inversion of magnetic induced polarization data, in J. Macnae and G. Liu, eds., ASEG, Three-dimensional electromagnetics III: 11p.
- Gasperikova, E. and Morrison, H. F., 2001, Mapping of induced polarization using natural fields: *Geophysics*, 66, 137-147.
- Haber, E. and Ascher, U. M., 2001, Fast finite volume simulation of 3d electromagnetic problems with highly discontinuous coefficients: *SIAM Journal on Scientific Computing*, 22, 1943-1961.
- Haber, E., Ascher, U. M. and Oldenburg, D. W., 2004, Inversion of 3D electromagnetic data in frequency and time using an inexact all-at-once approach: *Geophysics*, 69, 1216-1228.
- Hohmann, G. W., Kintzinger, P. R., Van Voorhis, G. D. and Ward, S. H., 1970, Evaluation of the measurement of induced electrical polarization with an inductive system: *Geophysics*, 35, 901-915.
- Kelley, C. T., 1999, *Iterative methods for optimization*: SIAM, Philadelphia.
- Li, Y. and Oldenburg, D. W., 2000, 3-D inversion of induced polarization data: *Geophysics*, 65, 1931-1945.
- Oldenburg, D. W. and Li, Y., 1994, Inversion of induced polarization data: *Geophysics*, 59, 1327-1341.
- Pelton, S. H., Ward, S. H., Hallof, P. G., Sill, W. R., and Nelson, P. H., 1978, Mineral discrimination and removal of inductive coupling with multifrequency IP: *Geophysics*, 43, 588-609.
- Seigel, H. O., 1959, Mathematical formulation and type curves for induced polarization: *Geophysics*, 24, 547-565.
- Seigel, H. O., 1974, The magnetic induced polarization (MIP) method: *Geophysics*, 39, 321-339.